ESTIMATES ON THE REACH OF THE POWDER PART OF AVALANCHES

Peter Gauer[1,*]

[1] *Norwegian Geotechnical Institute, Norway*

ABSTRACT: Avalanche observations from Norway, Austria and Switzerland, which distinguish between dense (fluidized) flow and powder part, are analyzed to obtain probability information about the reach of the powder part. The analysis suggests that the relative run-out distance of the powder part increases with increasing mean slope angle of the track. The data provide useful hints for avalanche practitioners about the reach and the corresponding probabilities of the powder part of avalanches.

Keywords: avalanche observations, powder part, hazard mapping

1. INTRODUCTION

Snow avalanches pose a deadly peril to human and a danger to their belongings. Avoidance of areas that can be impacted by avalanches is the most efficient mitigation measure. Thereby, hazard mapping is an important tool and practitioners are often confronted to assess the run-out distance and return period of dry-mixed avalanches; avalanches that are partially fluidized and accompanied by a powder cloud or air blast. The destructive effect of the suspension cloud or air blast can often be observed a considerable distance ahead of the more obvious deposits of the dense part of those avalanches. Fig. 1 shows examples of the impact signs of the powder cloud.

There is a long lasting interest in the destructive pressure wave from the powder cloud or air blast, respectively, and various explanations exist (e.g. Coaz, 1889; Sprecher, 1911; Bütler, 1937; Heinrich, 1956; Moskalev, 1975; Mellor, 1978). Also several expressions are linked to the phenomenon, for example, powder snow avalanche, air blast, wind blast, and in Norway 'skredvind'.

However, little is published about observations or measurements on the actual reach of the powder cloud. This paper presents some observations.

2. OBSERVATIONS FROM AVALANCHE

The analysis involves a series observations from major events (i.e. avalanches of the relative size R4 and R5 (Greene et al., 2016)) in which also the run-out distance of the a powder part was observed. The return period of those events is assumed to be in the order of 100 years.

Figure 1: Signs of "air blast" impacts: top) snow deposits and damage caused by the 'skredvind' of the powder snow avalanche from Stortuva, Mosjøen, Norway, on 29.02.1996 (photo NGI); bottom) building damage caused by the Meira powder snow avalanche, Arvigio, Switzerland, on 12.01.1977 (photo Canton police, Grisons)

2.1. Data

The data mainly consist of the avalanche path profile, the estimated position of the crown in the avalanche release zone, and the (estimated) position of the "maximum run-out". For the dense part this is typically marked by the tip of the obvious deposition. For the powder part the limit is somewhat scattered, but probably somewhere between the 1

*Corresponding author address:
Peter Gauer, Norwegian Geotechnical Institute,
P.O. Box 3930 Ullevl Stadion, NO–0806 Oslo, Norway
Tel: ++47 45 27 47 43; Fax: ++47 22 23 04 48; E-mail: pg@ngi.no

Table 1: Analyzed avalanche data.

Group	number	mean(Δz_b)* (m)	std(Δz_b) (m)	mean(β) (°)	std(β) (°)	estimated return period (years)	source
Norway	47	1031	270	36.4	7.1	30 – 300	(Haug, 1974) and others
Austria	59	999	328	28.5	5.7	100	(Klenkhart and Weiler, 1994)
Switzerland	6	844	185	30.9	2.1	–	(Förster, 1999; Issler et al., 1996)
total	112	988	294	31.9	7.3	–	

* Δz_b is the drop height from the top of the release area down to the β-point.

kPa and 3 kPa pressure limit; a pressure that still could cause noticeable damage at houses or vegetation.

For 59 data sets from Austria the run-out was clearly distinguished between dense (fluidized) flow and powder part. Most of the Norwegian data originate from Sunndal (Haug, 1974) or Møre & Romsdal area. For those data the so-called 'skredvind' was especially marked. In addition several data from Switzerland are included. Table 1 gives a brief overview of the data included in the analysis.

The mean drop height of the analyzed avalanches is around 988 m with a standard deviation of 294 m. Fig. 2 shows the α-angle of the dense part and the one for the reach of the powder part of the avalanches versus the β-angle. For comparison, the Norwegian relation of the well-known α-β (Lied and Bakkehøi, 1980) for mean the "Fahrböschungswinkel" ,

$$\alpha_m = 0.96\beta - 1.4^\circ\,, \tag{1}$$

is also included. The standard deviation of this relation, σ, is 2.3°. Gauer et al. (2010) derived a corresponding relation for the mean retarding acceleration,

$$\frac{a_r}{g} \approx 0.82\sin\beta + 0.05\,, \tag{2}$$

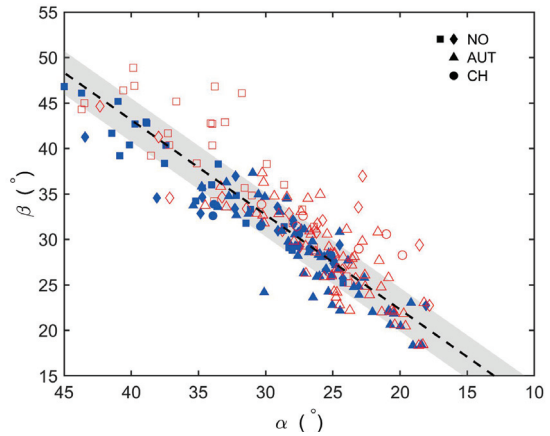

Figure 2: α-angle of the dense part (filled marker) and for the reach of powder part of the avalanches (open marker) versus the β-angle. The dashed line shows the fit Eq. (1) according to (Lied and Bakkehøi, 1980) and the gray-shaded area marks the corresponding-range.

with $\pm\sigma/g = 0.04$ and g is the gravitational acceleration.

2.2. Mean retarding acceleration

For the our analysis, we focus on the mean retarding acceleration of the dense and of the powder part. The effective retarding acceleration is a measure for the energy dissipation along the track and is given as

$$a_{r_i} = g\frac{\Delta z_i}{S_i}\,. \tag{3}$$

Here, Δz_i is the drop height from the top of the release area to the end of run-out area and S_i is distance along the track (arc-length). The subscript i marks either the dense part (DF) or the powder part (PSA).

Fig. 3 shows an example of an avalanche profile from the area around Hellesylt, Norway, and the mean retarding acceleration.

To describe the difference in run-out of dense part and the powder part, we focus the normalized difference between the mean retarding accelerations

$$\Delta a_{rn} = \frac{(a_{r_{PSA}} - a_{r_{DF}})}{a_{r_{DF}}}\,. \tag{4}$$

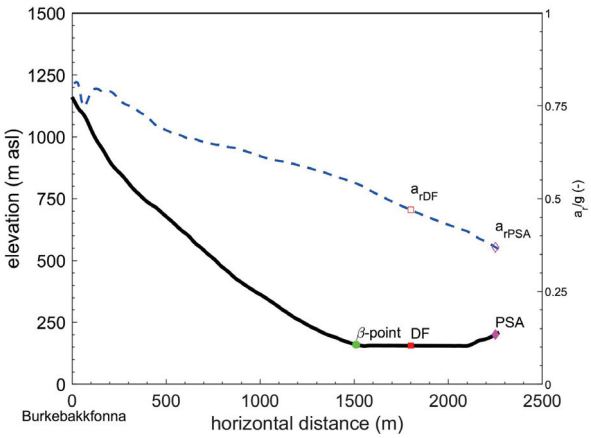

Figure 3: Avalanche profile of Burkebakkfonna, Møre & Romsdal, Norway. The β-point (Lied and Bakkehøi, 1980) and the run-out position of the dense part (DF) and the powder part (PSA) are indicated. In addition the mean retarding acceleration a_r, (see Eq. (3)), corresponding to a given horizontal stopping position is shown (dashed line). The markers indicate a_{rDF} and a_{rPSA} for the given example.

3. DISCUSSION

Fig. 4 shows the Δa_{rn} versus $\sin\beta$. Negative values imply longer run-out distance or uphill climbing of the powder part. Despite a considerable variation, there is a noticeable trend and the Spearman rank correlation between Δa_{rn} and $\sin\beta$ is -0.51. This suggests that difference of the run-out between the dense part and powder part increases with increasing mean slope angle. The trend is given by

$$\Delta a_{rf} \approx -0.23 \sin\beta + 0.06\,. \qquad (5)$$

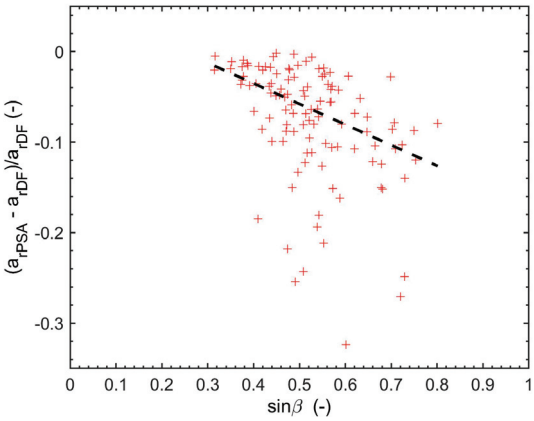

Figure 4: Δa_{rn} versus $\sin\beta$. The dashed line indicates the mean trend.

The boxplots in Fig. 5 show the remaining variation of the de-trended Δa_{rn}, that is

$$\sigma_\Delta = \Delta a_{rn} - \Delta a_{rf}\,. \qquad (6)$$

The figure shows both the variation of the combined data set and split into the three countries.

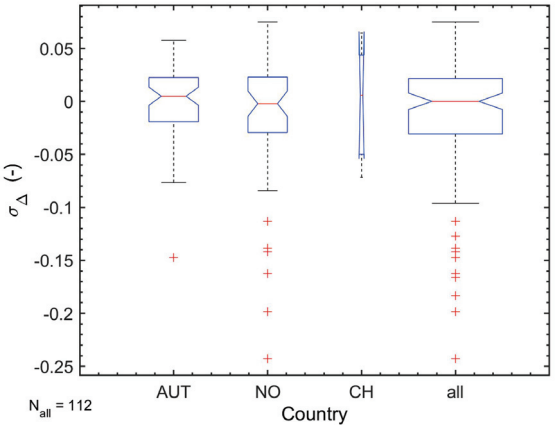

Figure 5: Boxplot of the variation σ_Δ. The median is shown by the red central mark, the 25th–75th percentile as edges of the blue box, the whiskers extend to the most extreme data points not considered outliers and outliers are marked with a red cross (points larger than $q_3+1.5(q_3-q_1)$ or smaller than $q_1-1.5(q_3-q_1)$, where q_1 and q_3 are the 25th and 75th percentiles). The notched area signifies a 95% confidence interval for the median and the width of the box indicates the relative size of the respective data set.

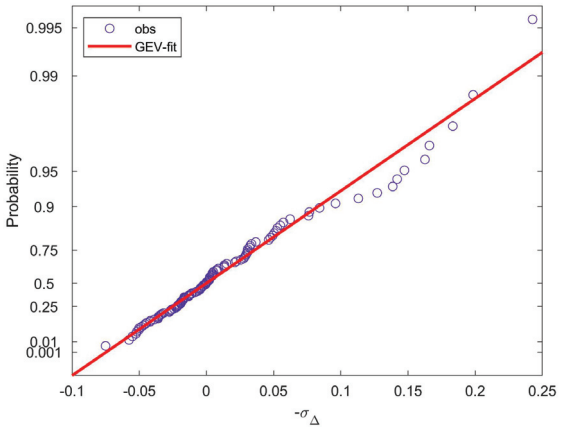

Figure 6: Probability plot of $-\sigma_\Delta$.

There is little difference in the median, which may suggest that the trend is similar in all data sets.

The variation of the combined data set, $-\sigma_\Delta$, may be approximated by a generalized extreme value distribution whose cumulative probability distribution is

$$\mathrm{CDF}(-\sigma_\Delta;\mu_p,\sigma_p,k_p) = \exp\left(-\left[1+k_p\left(\frac{-\sigma_\Delta-\mu_p}{\sigma_p}\right)\right]^{-1/k_p}\right), \qquad (7)$$

with a location parameter, $\mu_p \approx -0.0137$; scale parameter, $\sigma_p \approx 0.036$; and shape parameter, $k_p \approx 0.147$. Fig. 6 shows the corresponding probability plot.

Using (5) and (7) it is possible to obtain estimates on the exceedance probability of the ratio

$$\frac{a_{rDF}}{a_{rPSA}} = \frac{1}{1+\Delta a_{rn}}\,, \qquad (8)$$

depending on the mean slope angle β. For $\Delta z_{DF} \approx \Delta z_{PSA}$, this ratio is approximately S_{PSA}/S_{DF}. Fig. 7 shows the calculated ratio a_{rDF}/a_{rPSA} versus $\sin\beta$ for various exceedance probabilities. The figure also includes our example from Fig. 3.

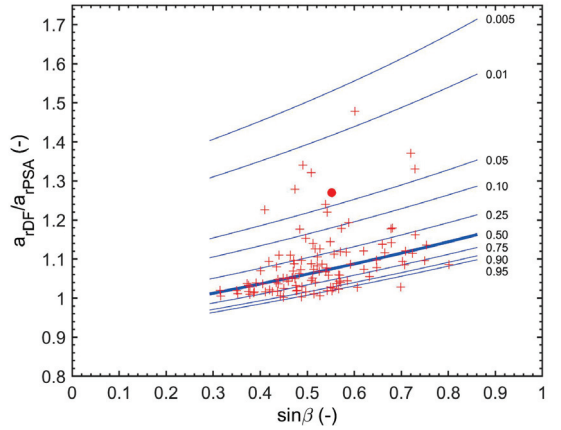

Figure 7: Ratio a_{rDF}/a_{rPSA} versus $\sin\beta$ for a given exceedance probability. The crosses show the observations and the bullet marks the example from Burkebakkfonna in Fig. 3.

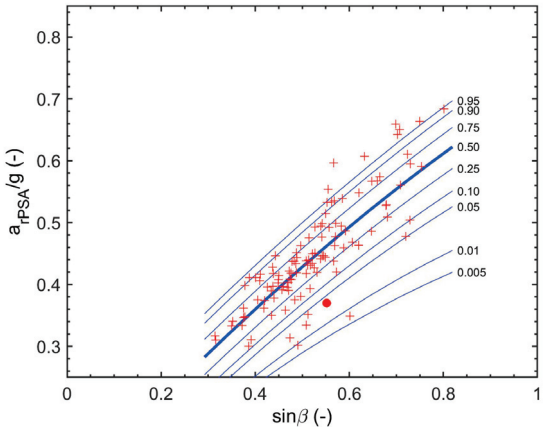

Figure 8: Estimated survival probability of mean retarding acceleration a_{rPSA}/g ($= \Delta z_{PSA}/S_{PSA}$) versus sinβ. The crosses show the observations and the bullet marks the example from Burkebakkfonna in Fig. 3.

A first estimate on the probability of the mean retarding acceleration of the powder part depending on the mean slope angle (and with that an estimate on its run-out distance) might be obtained by combining Eqs. (2) and (8). Fig. 8 shows the calculated survival probability of a_{rPSA}. For comparison the observation are included.

In similar manner, one could derive estimates on the probability of the "Fahrböschungswinkel" α. Fig. 9 shows the calculated survival probability of α_{PSA}. For comparison, relation (1) is included in the figure.

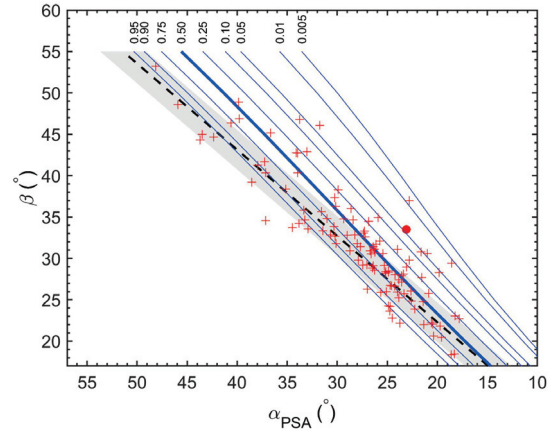

Figure 9: Estimated survival probability of α_{PSA} versus β. The crosses show the observations and the bullet marks the example from Burkebakkfonna in Fig. 3. For comparison, the dashed line shows the relation (1) and the gray-shaded area marks the corresponding $\pm\sigma$-range.

4. CONCLUDING REMARKS

Avalanche risk management requires knowledge of run-out distances and the corresponding return periods as well as intensity measures. At present, most avalanche models focus mainly on the prediction of the run-out distance of the dense- or fluidized-part, respectively. This holds true for the empirical models (Lied and Bakkehøi, 1980; McClung and Mears, 1991) as well as for the numerical models (Perla et al., 1980; Salm et al., 1990; Christen et al., 2010). This paper presents estimates of the ratio between the mean retarding acceleration of the dense part of an avalanche and the powder part depending on the mean slope angle of the track and a given exceedance probability. The knowledge of this ratio combined with an approximation of the run-out distance of the dense part can provide estimates on the reach of the powder part. The presented estimates are based on a limited set of data of around 100 avalanche observations from Norway, Austria and Switzerland with drop heights of around 1000 m. Nonetheless, they can provide useful hints for avalanche practitioners on the reach and the corresponding probability. In combination with the avalanche release probability of major events this gives information on the "return period" of an avalanche to reach a certain distance. The estimates on the reach may also help to evaluate results from numerical models.

ACKNOWLEDGMENTS

Parts of this research was financially supported by the Norwegian Ministry of Oil and Energy through the project grant R&D Snow avalanches 2017 - 2019 to NGI, administrated by the Norwegian Water Resources and Energy Directorate (NVE).

REFERENCES

Bütler, M. (1937). Zum Luftdruckproblem der Staublawinen. In *Die Alpen*, pages 464–465. SAC.

Christen, M., Kowalski, J., and Bartelt, P. (2010). RAMMS: Numerical simulation of dense snow avalanches in three-dimensional terrain. *Cold Regions Science and Technology*, 63:1–14.

Coaz, J. W. (1889). *Der Lawinenschaden im schweizerischen Hochgebirge im Winter und Frühjahr 188788*. Stämpfli.

Förster, M. (1999). Ausführliche Dokumentation ausgewählter Staublawinenereignisse und Bestimmung ihrer Eingangsparameter für die Verifikation von Staublawinenmodellen. Master's thesis, Mitt. Eidgenöss. Inst. Schnee- Lawinenforsch., Davos, Flüelastr 11., CH-7260 Davos.

Gauer, P., Kronholm, K., Lied, K., Kristensen, K., and Bakkehøi, S. (2010). Can we learn more from the data underlying the statistical α-β model with respect to the dynamical behavior of avalanches? *Cold Regions Science and Technology*, 62:42–54.

Greene, E., Atkins, D., Birkeland, K., Elder, K., Landry, C., Lazar, B., McCammon, I., Moore, M., Sharaf, D. Sternenz, C., Tremper, B., and Williams, K. (2016). Snow, Weather, and Avalanches: Observation Guidelines for Avalanche Programs in the United States. Technical report, American Avalanche Association.

Haug, J. M. (1974). Snøskred Registrering og Kartlegging innen Sunndal Kommune. Master's thesis, Universitetet i Oslo.

Heinrich, G. (1956). Gasdynamische Wirkungen von Staublawinen. *ZAMM - Journal of Applied Mathematics and Mechanics / Zeitschrift fr Angewandte Mathematik und Mechanik*, 36(7–8):298–300.

Issler, D., Gauer, P., Schaer, M., and Keller, S. (1996). Staublawinenereignisse im Winter 1995: Seewis (GR), Adelboden (BE) und Col du Pillon (VD). Interner Bericht 697, Eidgenöss. Inst. Schnee- Lawinenforsch., Davos, Flüelastr 11., CH-7260 Davos.

Klenkhart, C. and Weiler, C. (1994). Lawinen Technische Aufnahmen in den Bundesländern Vorarlberg, Tirol, Kärnten, und Salzburg. Technical report, Forsttechnischer Dienst für Wildbach und Lawinenverbauungen, Sektion Tirol, Innsbruck.

Lied, K. and Bakkehøi, S. (1980). Empirical calculations of snow-avalanche run-out distance based on topographic parameters. *Journal of Glaciology*, 26(94):165–177.

McClung, D. M. and Mears, A. I. (1991). Extreme value prediction of snow avalanche runout. *Cold Regions Science and Technology*, 19(2):163–175.

Mellor, M. (1978). *Dynamics of snow avalanches*, volume 14 of *Developments in Geotechnical Engineering*, chapter 23, pages 753–792. Elsevier Sci Ltd, New York.

Moskalev, Y. D. (1975). On the origin of wind blasts and air jets caused by the motion of avalanches. In Rodda, J., editor, *The International Symposium on Snow Mechanics, Grindelwald, Switzerland, April 1-5, 1974*, volume 114 of *IAHS Publ.*, page 381. Int. Assoc. Hydrol. Sci.

Perla, R., Cheng, T. T., and McClung, D. M. (1980). A two-parameter model of snow-avalanche motion. *Journal of Glaciology*, 26(94):119–207.

Salm, B., Burkard, A., and Gubler, H. U. (1990). Berechnung von Fliesslawinen. Eine Anleitung für Praktiker mit Beispielen. Mitt. Eidgenöss. Inst. Schnee- Lawinenforsch. 47, Eidgenöss. Inst. Schnee- Lawinenforsch., SLF, Davos, Switzerland.

Sprecher, F. W. (1911). Über die Mechanik der Staublawine. *Deutsche Alpenzeitung*, 11:241–249.